Dimers of mitochondrial ATP synthase induce membrane curvature and self-assemble into rows

Thorsten B. Blum[a,1], Alexander Hahn[a], Thomas Meier[a,2], Karen M. Davies[a,3], and Werner Kühlbrandt[a,4]

[a]Department of Structural Biology, Max Planck Institute of Biophysics, 60438 Frankfurt am Main, Germany

Edited by David J. DeRosier, Brandeis University, Waltham, MA, and approved January 3, 2019 (received for review September 25, 2018)

Mitochondrial ATP synthases form dimers, which assemble into long ribbons at the rims of the inner membrane cristae. We reconstituted detergent-purified mitochondrial ATP synthase dimers from the green algae *Polytomella* sp. and the yeast *Yarrowia lipolytica* into liposomes and examined them by electron cryotomography. Tomographic volumes revealed that ATP synthase dimers from both species self-assemble into rows and bend the lipid bilayer locally. The dimer rows and the induced degree of membrane curvature closely resemble those in the inner membrane cristae. Monomers of mitochondrial ATP synthase reconstituted into liposomes do not bend membrane visibly and do not form rows. No specific lipids or proteins other than ATP synthase dimers are required for row formation and membrane remodelling. Long rows of ATP synthase dimers are a conserved feature of mitochondrial inner membranes. They are required for cristae formation and a main factor in mitochondrial morphogenesis.

mitochondria | ATP synthase | membrane curvature | electron cryotomography | subtomogram averaging

Mitochondria play a central role in bioenergetics and cell physiology, as they generate most of the ATP in eukaryotes. Like their bacterial ancestors, mitochondria have an outer and an inner membrane. The inner membrane is folded into deep membrane invaginations called cristae. The cristae increase the inner membrane surface to accommodate large numbers of respiratory chain complexes and ATP synthase. Electron transfer through the respiratory chain is coupled to proton translocation from the matrix into the cristae lumen. The resulting electrochemical proton gradient across the inner membrane powers the production of ATP from ADP and phosphate by the ATP synthase.

The mitochondrial F_1F_o-ATP synthase consists of a ∼10-nm hydrophilic, ATP-generating F_1 head and the membrane-embedded F_o complex. Mitochondrial F-type ATP synthases differ from those of bacteria or chloroplasts in that they form dimers in the membrane (1). Dimer formation depends on protein subunits (2–4) that are absent in the prokaryotic or chloroplast ATP synthases (5). The first indication that mitochondrial ATP synthase forms dimers came from blue-native gel electrophoresis (2). Subsequently, it was shown that the dimer-specific subunits *e* and *g* of yeast ATP synthase were required for cristae formation (6, 7), establishing a link between ATP synthase dimers and inner membrane morphology. Electron microscopy of negatively stained protein complexes extracted from blue-native gels indicated that dimers were V-shaped (8), and it was proposed that they bend the membrane and contribute to cristae formation (9, 10). Rows of particles that were thought to be ATP synthase dimers were first observed in deep-etched tubular cristae of *Paramecium* (11). Later, ATP synthase dimer rows were discovered by electron cryotomography (cryo-ET) in inner membrane fragments from bovine (12), yeast (13), and *Polytomella* mitochondria (14). Cryo-ET of inner mitochondrial membranes from plants (13), ciliates (15), and flagellates (16) has revealed long rows of ATP synthase dimers along the strongly curved edges of the lamellar cristae or helical tubular cristae, suggesting that the rows are an ubiquitous, conserved feature of all mitochondria. The rows extend for hundreds of nanometers, with dozens of dimers arranged side by side. The two F_1F_o complexes in a dimer include angles ranging from 70° to 90° (12, 13), resulting in characteristic dimer shapes that vary between eukaryotic clades.

Recently, the structures of isolated, detergent-solubilized ATP synthase dimers from mitochondria of the yeast *Yarrowia lipolytica* and the green alga *Polytomella* have been determined by single-particle cryo-EM at 6.2-Å (17) and 3.7-Å (18) resolution. The structures of the F_o dimer without F_1 heads and of the monomeric F_1F_o-ATP synthase from the yeast *Saccharomyces cerevisiae* have both been reported at 3.6-Å resolution (4, 19).

Molecular simulations have suggested that ATP synthase dimer rows bend the membrane locally, and that the induced membrane curvature promotes row formation (3, 20). We now provide experimental proof that ATP synthase dimers of two different types do indeed assemble into rows and bend the membrane. Purified ATP synthase dimers or monomers reconstituted with membrane lipids into proteoliposomes were examined by cryo-ET and subtomogram averaging. Results

Significance

The ATP synthase in the inner membrane of mitochondria generates most of the ATP that enables higher organisms to live. The inner membrane forms deep invaginations called cristae. Mitochondrial ATP synthases are dimeric complexes of two identical monomers. It is known that the ATP synthase dimers form rows along the tightly curved cristae ridges. Computer simulations suggest that the dimer rows bend the membrane locally, but this has not been shown experimentally. In this study, we use electron cryotomography to provide experimental proof that ATP synthase dimers assemble spontaneously into rows upon membrane reconstitution, and that these rows bend the membrane. The assembly of ATP synthase dimers into rows is most likely the first step in the formation of mitochondrial cristae.

Author contributions: T.B.B., K.M.D., and W.K. designed research; T.B.B. and A.H. performed research; T.B.B., A.H., T.M., K.M.D., and W.K. analyzed data; and W.K. wrote the paper.

The authors declare no conflict of interest.

This article is a PNAS Direct Submission.

[1]Present addresses: Department of Biology and Chemistry, Paul Scherrer Institut (PSI), CH-5232 Villigen PSI, Switzerland; and Center for Cellular Imaging and NanoAnalytics (C-CINA), Biozentrum, University of Basel, CH-4058 Basel, Switzerland.

[2]Present address: Department of Life Sciences, Imperial College London, SW7 2AZ London, United Kingdom.

[3]Present addresses: Molecular Biosciences and Integrated Bioimaging, Lawrence Berkeley National Laboratory, Berkeley, CA 94720; and Department of Molecular and Cell Biology, University of California, Berkeley, CA 94720.

[4]To whom correspondence should be addressed. Email: werner.kuehlbrandt@biophys.mpg.de.

This article contains supporting information online at www.pnas.org/lookup/suppl/doi:10.1073/pnas.1816556116/-/DCSupplemental.

Published online February 13, 2019.

demonstrate that ATP synthase dimers distort the flat lipid bilayer and form rows, without the participation of other proteins. By contrast, ATP synthase monomers are randomly distributed in the reconstituted liposomes, do not form rows, and do not induce long-range membrane curvature.

Results

ATP Synthase Dimers Form Rows in *Polytomella* Mitochondria. The outer and inner membranes of mitochondria isolated from *Polytomella* sp. are readily visible as dark lines in slices of tomographic volumes. At a resolution of ~3 nm, the outer membrane appears smooth and featureless. It is separated from the inner boundary membrane by a 20-nm gap of intermembrane space (Fig. 1). The inner membrane is deeply invaginated into the inner membrane cristae. The cristae are densely studded with double rows of ATP synthase dimers (Fig. 1*A*). Subtomogram averages of dimer rows from broken cristae membranes (*SI Appendix*, Fig. S1) indicate an average interdimer distance of 13.4 nm and a lateral offset of 2.9 nm between adjacent dimers in a row. Rendered volumes indicate that the dimers are arranged in rows that wrap around the edges of the cristae, which in *Polytomella* tend to be club-shaped (Fig. 1 *B* and *C*). The inner boundary membranes and the flat membrane regions between the cristae edges are devoid of dimers. Cryo-ET did not reveal monomeric ATP synthase in any part of the inner membrane.

ATP Synthase Dimers Induce Membrane Curvature. Detergent-solubilized dimers were purified from mitochondrial membranes of *Polytomella* sp. or *Y. lipolytica* by column chromatography and density gradient centrifugation. Dimers were reconstituted into proteoliposomes by the GRecon method (21). The solubilized protein solution was placed onto a linear glycerol gradient containing partly solubilized liposomes and cyclodextrin. Upon centrifugation, the protein migrates into the gradient, detergent is absorbed by cyclodextrin, while the dimers incorporate into the liposomes. Reconstituted vesicles migrate to different gradient positions, depending on their protein content. With reconstituted *Polytomella* dimers, two proteoliposome bands were usually observed, one with low protein content at a gradient density of 1.09 g/L (high lipid-to-protein ratio) and one with higher protein content (low lipid-to-protein ratio) at 1.13 g/L (*SI Appendix*, Figs. S2 and S3).

Polytomella proteoliposomes from the lower, heavier gradient fraction (Fig. 2*A*) varied in shape and size. Membranes were densely packed with ATP synthase dimers (Fig. 2 *B* and *C*). Dimer insertion into the membrane appeared to be mostly bidirectional, except in small vesicles with high positive curvature (convex as seen from the outside), into which dimers tended to insert unidirectionally, with their F_1 heads pointing out of the vesicle. Occasionally, dimers incorporated in the opposite orientation, so that their F_1 heads pointed into the vesicle interior (Fig. 2*D*). In this case, the local membrane curvature was inverted (concave as seen from the outside), demonstrating that individual dimers impose a defined, high local curvature on the membrane.

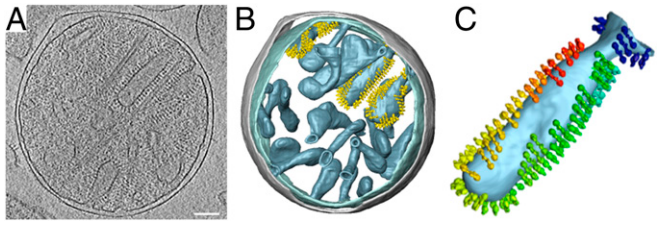

Fig. 1. Cryo-ET of isolated *Polytomella* sp. mitochondria. (*A*) Tomographic volume showing inner membrane cristae studded with ATP synthase dimers surrounded by the smooth, featureless outer membrane. (*B*) Segmented volumes show ATP synthase dimers arranged in rows. All cristae vesicles are similarly populated, but for clarity, ATP synthase dimers are shown in only three of them. Inner membrane, light blue; outer membrane, gray; ATP synthase dimers, yellow. (*C*) Individual club-shaped crista. Dimers in the membrane are replaced by subtomogram average volumes (rainbow colors). Dimer rows wrap around the tightly curved cristae edges. (Scale bar, 100 nm.)

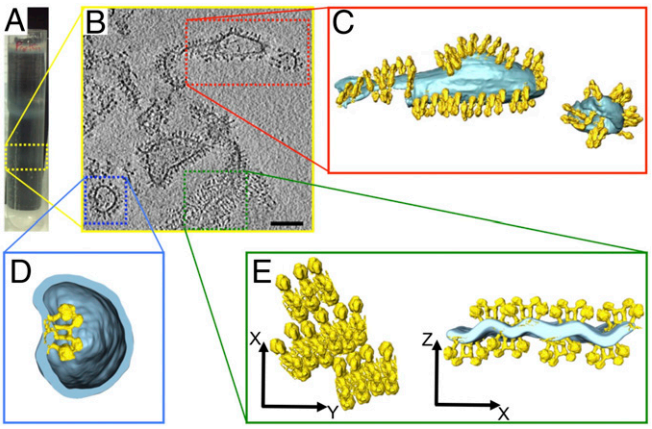

Fig. 2. *Polytomella* sp. ATP synthase dimers reconstituted at low lipid/protein ratio. (*A*) The lower gradient band (dashed yellow box) contains proteoliposomes with high protein density. (*B*) Cryo-ET indicates irregular vesicle shapes and membrane fragments densely packed with ATP synthase dimers. (Scale bar, 100 nm.) (*C–E*) Segmented tomographic volumes. (*C*) Reconstituted ATP synthase dimers (yellow) form rows in the membrane (light blue). (*D*) Occasionally dimers insert with their F_1 heads pointing into the vesicle, indicating that individual dimers impose local membrane curvature. (*E*) Membrane region with parallel ATP synthase dimer rows. The cross-section (*Right*) reveals that rows on opposite sides of the membrane distort the lipid bilayer into a corrugated sheet. *C*, *D*, and *E* are not on the same scale.

ATP Synthase Dimers Self-Assemble into Rows. In larger *Polytomella* proteoliposomes taken from the heavier gradient fraction, the dimers formed rows that closely resembled those in the club-shaped *Polytomella* cristae (Fig. 1 *B* and *C*), except that dimer ribbons were observed on either side of the reconstituted lipid bilayer, due to bidirectional insertion. Some ribbons associated into rafts of parallel rows (Fig. 2*E*). Cross-sections perpendicular to the ribbon direction revealed that each row bent the lipid bilayer to a similar degree as individual dimers (Fig. 2*D*). In the rafts, rows on both sides of the membrane shaped the lipid bilayer into a corrugated sheet (Fig. 2*E*). Bending angles at the ridges were estimated at 128 ± 10°, indicating that the 56° angle between the central stalks of the two F_1F_o complexes in the *Polytomella* dimer (18, 22) induced a corresponding, roughly (180–56°) curvature of the lipid bilayer.

Polytomella proteoliposomes from the lighter, lipid-rich gradient fraction (Fig. 3*A*) tended to be spherical. The lipid bilayers of these vesicles were mostly empty (Fig. 3*B*), but every time a protein density was detected in the membrane, it was a V-shaped ATP synthase dimer. Most of the dimers had associated into ribbons around the vesicle perimeter (Fig. 3*C*). With few exceptions, the F_1 heads pointed out of the vesicles into the surrounding medium (Fig. 3*D*), indicating that membrane insertion at high lipid-to-protein ratio was predominantly unidirectional. Cross-sections perpendicular to the ribbons revealed that the dimer rows bent the lipid bilayer to the same degree as individual dimers (Fig. 2*D*) or rafts (Fig. 2*E*).

Proteoliposomes of reconstituted *Y. lipolytica* ATP synthase dimers usually formed only one band on the gradient. Vesicles assumed a range of irregular shapes, including flattened disks, square tubes and corrugated sheets (Fig. 4). Membrane insertion was either unidirectional (Fig. 4 *A* and *B*) or bidirectional (Fig. 4

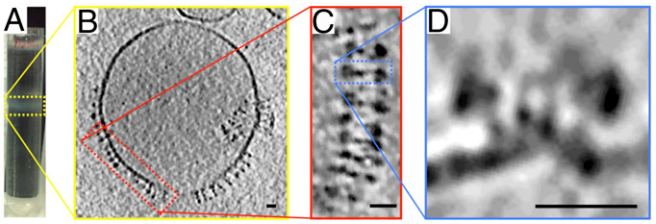

Fig. 3. *Polytomella* sp. ATP synthase dimers reconstituted at high lipid/protein ratio. (*A*) The upper gradient band (yellow box) contains proteoliposomes with low protein density. (*B*) Cryo-ET of low-density vesicles indicates that the membrane is mostly empty and reconstituted dimers assemble into long rows (red box). (*C*) Consecutive dimers are laterally offset as in *Polytomella* cristae (Fig. 1*C*). (*D*) Cross-sections (blue box) reveal that rows bend the membrane locally. A subtomogram average of reconstituted dimer rows is shown in *SI Appendix*, Fig. S1. (Scale bars, 20 nm.)

C and *D*). The dimers were always arranged in rows along the highly curved vesicle edges or ridges of corrugated sheets, whereas flat membrane regions were unpopulated (Fig. 4 *A* and *B*). As observed for *Polytomella*, parallel dimer ribbons occasionally assembled into rafts, in which the lipid bilayer was bent into a pleated sheet (Fig. 4 *C* and *D*). Folding angles at the ridges were close to 90°, reflecting the 86° dimer angle of *S. cerevisiae* (3) or *Y. lipolytica* ATP synthase (17). Consecutive tomographic slices perpendicular to the rows show that the bending angle persists throughout the length of a dimer ribbon (Movies S1 and S2). The rows were usually longer than those observed in *Polytomella*. The typical distance between adjacent dimers in a ribbon was ∼12 nm, as in tomograms of inner membrane fragments from bovine heart (12) or yeast mitochondria (3).

Isolated and Reconstituted ATP Synthase Dimers Have the Same Structure. The structure of ATP synthase dimers from *Polytomella* sp. (Fig. 5*A*) or *Y. lipolytica* (Fig. 5*B*) reconstituted into proteoliposomes was determined by subtomogram averaging to an estimated resolution of ∼29 Å (Fig. 5*C*). The two leaflets of the lipid bilayer were resolved. The average volumes agree closely with the higher-resolution single-particle structures of detergent-solubilized *Polytomella* (18, 22) and *Y. lipolytica* dimers (17). In particular, the angles between the central axes of the two F_1F_o complexes in the dimers (56° in *Polytomella*; 86° in *Y. lipolytica*) agree with the dimer angles observed by single-particle cryo-EM and by subtomogram averaging of dimers in cristae membrane fragments (3). Detergent solubilization and membrane reconstitution hence do not change the structure of the dimeric assemblies visibly at this resolution.

Reconstituted ATP Synthase Monomers Do Not Form Rows. ATP synthase dimers from *Y. lipolytica* treated with the nonionic detergent dodecyl maltoside (DDM) dissociate into monomers and lose the dimer-specific subunits *e*, *g*, and *k* (17), whereas under the same conditions, the stable *Polytomella* dimer remains intact. DDM-solubilized *Y. lipolytica* monomers were reconstituted into proteoliposomes by the GRecon method. Cryo-ET revealed that ATP synthase monomers did not induce long-range membrane curvature, nor did they associate into rows (Fig. 6). This confirms our earlier observation that ATP synthase monomers lacking the dimer-specific subunits do not bend the detergent micelle, whereas the dimers do (17). The results demonstrate that the dimers themselves are directly responsible for bending the lipid bilayer at the ATP synthase dimer rows. The up or down orientation of ATP synthase monomers in larger vesicles was random (Fig. 6 *A*–*D*). In small, spherical vesicles, membrane insertion was unidirectional, with the F_1 heads pointing out of the vesicles (Fig. 6 *D* and *E*).

In summary, we conclude that (*i*) mitochondrial ATP synthase dimers reconstituted into proteoliposomes impose a local curvature on the lipid bilayer; (*ii*) reconstituted dimers self-assemble into ribbons; (*iii*) the ribbons run along membrane ridges of a curvature governed by the dimer angle; (*iv*) reconstituted dimer ribbons closely resemble those in native inner membrane cristae; (*v*) the structure of ATP synthase dimers in lipid bilayers is not affected by detergent solubilization and membrane reconstitution; and (*vi*) row formation and long-range membrane curvature depends on ATP synthase dimers, as monomers do not form rows.

Discussion

ATP Synthase Dimers in One Species Are Invariant. ATP synthase dimers of *Polytomella* sp. and *Y. lipolytica* have distinctly different molecular structures (Fig. 5) (17, 18). ATP synthase dimers from *Polytomella* sp. are particularly stable due to a protein bridge connecting the two peripheral stalks (18, 22), whereas yeast or mammalian dimers that lack this bridge dissociate more easily into monomers. *Polytomella* sp. dimers were purified in DDM, a mild, nonionic detergent. The less stable dimers from *Y. lipolytica* were purified in the very mild, natural detergent digitonin. When purified in DDM, the *Y. lipolytica* ATP synthase broke up into monomers within a few hours. The monomers were used for control experiments.

Two-dimensional projection images of isolated, detergent-solubilized bovine or yeast ATP synthase dimers in negative stain have suggested at least two populations with different dimer angles (8, 10, 23, 24). The different angles were thought to derive from monomer–monomer interactions either across the rows (dimer angle >70°) or along the rows (<40°) (10). The *Polytomella* and *Y. lipolytica* dimers reconstituted into liposomes were essentially the same as those we had used for high-resolution structure determination by single-particle cryo-EM (17, 18, 22). Our results show that the dimer structure in each species is invariant, irrespective of how it had been obtained (e.g., single-particle cryo-EM, subtomogram averaging of dimers in native mitochondrial membranes, or of dimers reconstituted into proteoliposomes) (Fig. 5). Some of the previously reported structures (8, 10, 23,

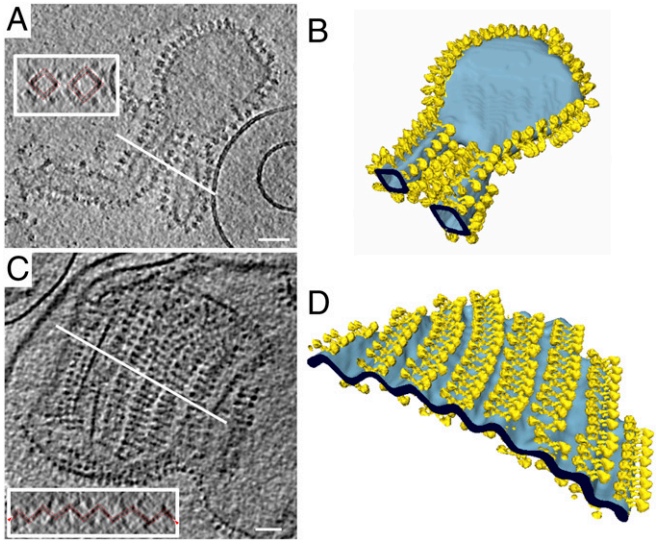

Fig. 4. Proteoliposomes of reconstituted *Y. lipolytica* ATP synthase dimers. (*A* and *C*) ATP synthase dimers (yellow) form rows that bend the lipid bilayer (light blue). *Insets* shows cross-sections (white lines), indicating that dimer rows bend the lipid bilayer by ∼90° (dashed red lines). (*B*) Flat membrane regions are devoid of ATP synthase. (*D*) Parallel rows of bidirectionally inserted dimers bend the bilayer into a corrugated sheet. (Scale bars, 100 nm.)

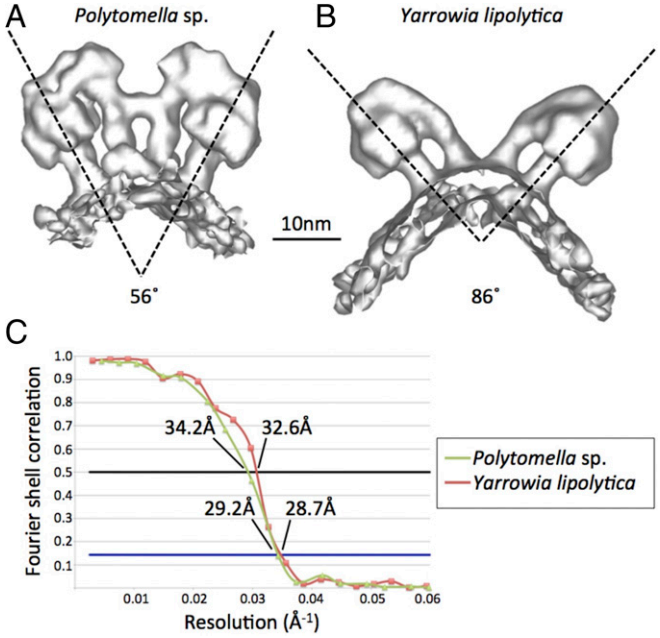

Fig. 5. Subtomogram average volumes of ATP synthase dimers. (*A*) *Polytomella* (average of 103 dimer volumes). (*B*) *Y. lipolytica* (158 dimer volumes). Dimer angles between central stalks are indicated. (*C*) Gold-standard Fourier shell correlation (FSC) curves for the 3D reconstructions indicate a resolution of ~29 Å at FSC = 0.143.

24) were thus either different 2D projections of the same dimer, or artifacts generated by random association of isolated monomers.

ATP Synthase Dimers Are Required for Row Formation. *S. cerevisiae* mutants lacking ATP synthase subunit *g* do not form dimers, as subunits *g* and *e* are required for dimerization (2, 25). ATP synthase monomers of these mutants are randomly distributed in the membrane (3). Their inner mitochondrial membranes do not develop lamellar cristae but single or multiple balloon-shaped vesicles. ATP synthase dimers are thus a prerequisite for row formation in vitro and for the formation of cristae in vivo.

Recent single-particle cryo-EM structures of the *Y. lipolytica* F_1F_o dimer (17) and of the *S. cerevisiae* F_o dimer (4) indicate that the interactions of subunits *e*, *g*, and *k* and the N-terminal transmembrane helix of subunit *a* together with subunit *i* (also known as *j*) result in the striking V-shape of the dimer, which we now show to be responsible for row formation. Bovine heart ATP synthase monomers that contain *e* and *g* distort the detergent micelle surrounding F_o (26), whereas yeast monomers that lose these subunits upon dissociation of the dimer do not (17). ATP synthase monomers do not form rows, because the membrane curvature they induce is small and lacks directionality. Row formation depends on unequal membrane curvature in two mutually perpendicular directions (3)

Although subunits *e* and *g* barely contribute to direct monomer contacts, they stabilize the dimer. The two subunits are essential for the formation of native ATP synthase dimers in the membrane, and hence for the formation of dimer rows and mitochondrial cristae (3). Note that dimers in the 2D membrane crystals of bovine F_1F_o (27) differ from native dimers, because monomers insert randomly, i.e., bidirectionally, into the reconstituted bilayer, whereas they assemble in only one orientation in the mitochondrial inner membrane.

Row Formation Does Not Depend on Particular Protein Subunits or Lipids. Molecular dynamics simulations suggest that a single *S. cerevisiae* ATP synthase dimer can deform planar lipid bilayers of POPC (1-palmitoyl-2-oleoyl-*sn*-glycero-3- phosphocholine) (3). When two or more ATP synthase dimers approach one another, they are likely to stay together, due to the reduction in elastic bending energy that distorts the planar lipid bilayer around each dimer. The directionality of the bending energy gives rise to an attractive force that results in row formation (20). This mechanism is highly effective; in our reconstitution assays, rows of 25 or more ATP synthase dimers were regularly observed (Figs. 2*B*, 3*B*, and 4), and few if any dimers were not part of a row. Rows can extend for several microns as they bend around the edges of disk-shaped proteoliposomes (Fig. 4 *A* and *B*) or cristae. The variable interdimer distance along rows of fungal or mammalian ATP synthases is consistent with the absence of specific protein-protein interactions and a high degree of flexibility. Row formation is unlikely to depend on the membrane lipid composition, since all biological membranes are fluid and ATP synthase dimers would bend them in the same way.

ATP Synthase Dimer Ribbons Define the Shape of Cristae. The liposomes used in our reconstitution experiments were inherently quasispherical, but large enough to consider the membrane as approximately flat at the scale of ATP synthase dimers. The observation that dimer rows form spontaneously in these liposomes therefore demonstrates that a preexisting membrane curvature is not required for the self-association of dimers. On the contrary, we observe that the rows have a profound influence on liposome morphology. Indeed, our tomograms of *Y. lipolytica* proteoliposomes reveal flattened disk-shaped vesicles (Fig. 4*B*) that bear a close resemblance to cristae vesicles isolated from fragmented bovine heart (12) or *S. cerevisiae* mitochondria (3). Proteoliposomes with reconstituted *Polytomella* dimers (Fig. 2*C*) resemble the club-shaped cristae in whole *Polytomella* mitochondria (Fig. 1*B*). The tubular cristae of ciliates appear to owe their structure to helical ribbons of U-shaped ATP synthase dimers (15). We conclude that the geometry of ATP synthase dimer ribbons is a main factor in determining cristae shape and mitochondrial inner membrane morphology.

Cristae are successive infoldings of the inner mitochondrial membrane. Membrane invagination is driven by lipid biosynthesis and the concomitant increase in membrane surface. As it expands

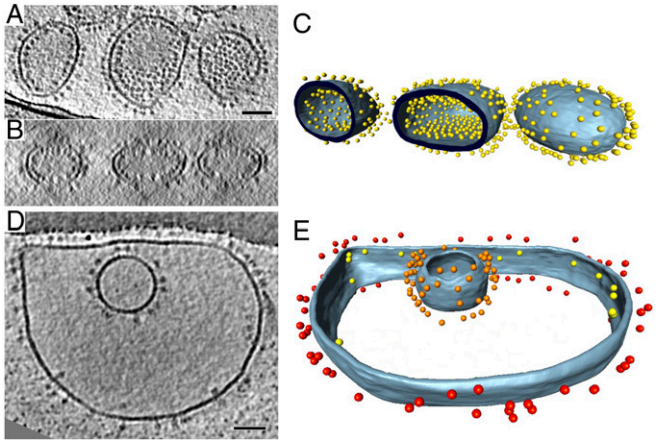

Fig. 6. Liposomes reconstituted with *Y. lipolytica* ATP synthase monomers. (*A* and *B*) Tomographic slices of liposomes reconstituted with different concentrations of monomeric ATP synthases from *Y. lipolytica*. (*C* and *E*) Segmented volumes of *A* and *D*. Blue-gray, membrane; colored spheres, ATP synthases. (*B*) Colors represent ATP synthase F_1 heads on different membrane surfaces. Red, outside of large outer vesicle; yellow, inside of large outer vesicles; orange, outside of small inner vesicle. Lipids are *E. coli* phosphatidyl ethanolamine (PE) 67%, phosphatidyl glycerol (PG) 23.2%, cardiolipin 9.8%. Percentages are in weight per volume. (Scale bar, 50 nm.)

within the confines of the outer membrane, the inner membrane buckles inward. Evidently, this process alone cannot account for the variable morphologies of cristae. Mathematical modeling indicates that, although multiple buckling events are likely to occur initially, membrane fusion would eventually result in several large, vesicle-like inner-membrane compartments (28, 29). It thus appears to be part of the biological role of the ATP synthase dimer rows to prevent this kind of vesiculation and to promote the formation of flat lamellar (or tubular) cristae. Presumably, rows of ATP synthase dimers assemble at multiple points in the inner membrane, priming these sites for invagination. As the membrane surface increases, the inner membrane preferentially buckles at these primed locations. ATP synthase dimer rows around the edges of growing cristae would prevent uncontrolled fusion, resulting in a large increase of membrane surface area. Mitochondria in tissues with a high demand for ATP, such as cardiac muscle, are packed with lamellar cristae at a stacking distance of ∼40 nm (30), increasing the surface of the inner membrane available for oxidative phosphorylation by a factor of 10 or more (1). In the confined volume of the cristae lumen, the lateral pH gradient along the membrane from the proton pumps of the respiratory chain (31) to the ATP synthase dimer rows may favor effective ATP synthesis.

Methods

Polytomella Culture. *Polytomella* sp. was grown in low light at room temperature without shaking. A 10-mL preculture was grown for 3 d in MAP buffer (30 mM Na acetate, 35 mM Mes, 0.8 mM K_2HPO_4, 0.2 mM KH_2PO_4, 7.4 mM NH_4Cl, 0.3 mM $CaCl_2$, 0.5 mM $MgSO_4$, 1.39 μm $ZnSO_4$, 0.8 μM H_3BO_3, 2.65 μM $MnSO_4$, 0.74 μM $FeCl_3$, 0.83 μM $NaMoO_4$, 0.16 μM $CuSO_4$, 0.6 μM KI; adjusted to pH 5.8 with 5 M KOH); 1 mL of preculture was added to each of seven 1-L Fernbach flasks containing 1 L of MAP medium. Cultures were grown for 3 d (32).

Mitochondria were isolated at 4 °C (33) with modifications. Cells were harvested by centrifugation at 10,500 × *g* for 15 min and resuspended in homogenization buffer [20 mM Mops-NaOH (pH 7.4), 250 mM sucrose, 1 mM EGTA, 0.3% (wt/vol) BSA, 1 tablet of Complete Protease Inhibitor Mixture] at a final volume of 50 mL. Cells were broken mechanically by 60 strokes of a 50-mL Teflon-glass potter (1,000 rpm), diluted to 180 mL with washing buffer [20 mM Mops-NaOH (pH 7.4), 250 mM sucrose, 1 mM EGTA] and centrifuged twice at 600 × *g* and 1,000 × *g* for 15 min. Mitochondria were pelleted at 12,000 × *g* for 15 min, washed twice with washing buffer at 12,000 × *g* for 15 min, resuspended to a concentration of 5–10 mg/mL, frozen in liquid nitrogen, and stored for further use at −80 °C.

ATP Synthase Purification. All steps were carried out at 4 °C. Aliquots of unfrozen *Polytomella* mitochondria were pelleted (21,000 × *g*, 15 min), resuspended in buffer A [31.2 mM Tris, 8.8 mM Mops (pH 8.8), 2 mM $MgSO_4$] to a concentration of 10 mg/mL and repelleted (21,000 × *g*, 15 min). The pellet was resuspended in buffer A to a concentration of 20 mg/mL, diluted with 4% DDM to 10 mg/mL in buffer B (15.6 mM Tris; 4.4 mM Mops; 1 mM $MgSO_4$; pH 8.8; 2% DDM). The solution was agitated for 30 min, and unsolubilized material was removed by centrifugation (13,000 × *g*, 15 min).

The supernatant of solubilized *Polytomella* membranes was partially purified by weak ion-exchange chromatography; 1 mL of wet diethylaminoethyl (DEAE) (Bio-Rad) resin was washed with 10 mL of water, activated with 10 mL of 500 mM NaCl, washed with 10 mL of water, and equilibrated with 10 mL of buffer C [15.6 mM Tris, 4.4 mM Mops (pH 8.8), 1 mM $MgSO_4$, 0.05% (wt/vol) EDTA]; 10 mg of detergent-solubilized protein was added to the column and incubated for 30 min at 4 °C. Unbound protein was removed by washing with six volumes of buffer C. ATP synthase dimers were eluted with buffer D [15.6 mM Tris, 4.4 mM Mops (pH 8.8), 1 mM $MgSO_4$, 0.05% (wt/vol) EDTA, 80 mM NaCl]. Finally, the column was washed with 10 volumes of water and 2 volumes of 20% (vol/vol) ethanol and stored at 4 °C.

Polytomella ATP synthase dimers were purified further by size-exclusion chromatography on a Superose 6 10/300 GL column with an ÄKTA purifier (GE Healthcare) at a constant flow rate of 300 μL/min. All buffers were filtered and degassed before use.

ATP synthase dimers and monomers from *Y. lipolytica* were purified as described (17).

ATP Synthase Reconstitution. ATP synthase was reconstituted into liposomes by the GRecon method (21) (*SI Appendix*, Fig. S2). Destabilized liposomes were obtained by sonicating 1.5 mg of *Escherichia coli* polar lipids (Avanti) in 150 μL of distilled H_2O with 1% (vol/vol) Triton X-100 for 30 min. Linear sucrose gradients were prepared with a gradient maker (86°, 20 rpm, 57 s; BioComp gradient Master Model 106) with 2 mL of buffer E [*Polytomella*: 0.3 M sucrose, 25 mM Tris•HCl (pH 7.8), 100 mM NaCl, 1 mM $MgCl_2$; *Y. lipolytica*: 0.3 M sucrose, 30 mM Mops-NaOH (pH 7.5), 2 mM $MgCl_2$, 0.5 mM EDTA] and 2 mL of buffer F [*Polytomella*: 1.3 M sucrose, 25 mM Tris•HCl (pH 7.8), 100 mM NaCl, 1 mM $MgCl_2$, 0.6 mg/mL destabilized liposomes, and 0.5 mg of α-cyclodextrin per mg DDM; *Y. lipolytica*: 1.3 M sucrose, 30 mM Mops-NaOH (pH 7.5), 2 mM $MgCl_2$, 0.5 mM EDTA, 0.6 mg/mL destabilized liposomes, and 0.5 mg of γ-cyclodextrin per mg digitonin].

A total of 1 mg of ATP synthase dimers or 0.5 mg of ATP synthase monomers were layered onto the gradient and centrifuged at 150,000 × *g* for 18 h at 4 °C in a SW60 rotor. After centrifugation, opaque bands containing liposomes were extracted from the gradient and washed twice in 2 mL of buffer [*Polytomella*: 50 mM Tris•HCl (pH 8.0), 1 mM $MgCl_2$; *Y. lipolytica*: 30 mM Mops-NaOH (pH 7.5), 2 mM $MgCl_2$, 0.5 mM EDTA].

Cryo-ET and Subtomogram Averaging. Cryo-ET was performed as described (34); 3 μL of proteoliposomes mixed 1:1 with fiducial markers (6-nm gold particles conjugated to protein A; Aurion) were applied to glow-discharged Quantifoil grids (R2/2, Cu 300 mesh; Quantifoil), blotted with no. 4 Whatman paper for 3 s to remove excess liquid, and plunge-frozen in liquid ethane with a home-built guillotine. Single-axis tilt series (±60°) were collected on an FEI Krios transmission electron microscope operating at 300 kV with a postcolumn energy filter (GIF Quantum; Gatan) and K2 summit detector operating in counting mode (Gatan). Tilt series were acquired with the software Latitude (Gatan) at a specimen pixel size of 0.34 (*Polytomella*) or 0.43 nm (*Y. lipolytica*) and a defocus of 3.5–6 μm. Tilt series were aligned using the gold fiducial markers and back-projected to generate tomographic volumes with the software IMOD (35). ATP synthase dimers were averaged as described (3) and repositioned into tomographic volumes with the AMIRA EM toolbox (36). Membranes were manually segmented in AMIRA (FEI).

ACKNOWLEDGMENTS. We thank Deryck Mills for running the cryo-EM facility and EM maintenance and Özkan Yildiz and Juan Francisco Castillo Hernandez for computer support. This work was supported by the Max Planck Society, the Collaborative Research Center Sonderforschungsbereich 807 of the Deutsche Forschungsgemeinschaft (DFG) (A.H. and T.M.) and the DFG-funded Cluster of Excellence Frankfurt "Macromolecular Complexes" (K.M.D. and W.K.).

1. Kühlbrandt W (2019) Structure and mechanisms of F-type ATP synthases. *Annu Rev Biochem* 88, in press.
2. Arnold I, Pfeiffer K, Neupert W, Stuart RA, Schägger H (1998) Yeast mitochondrial F_1F_0-ATP synthase exists as a dimer: Identification of three dimer-specific subunits. *EMBO J* 17:7170–7178.
3. Davies KM, Anselmi C, Wittig I, Faraldo-Gómez JD, Kühlbrandt W (2012) Structure of the yeast F_1F_o-ATP synthase dimer and its role in shaping the mitochondrial cristae. *Proc Natl Acad Sci USA* 109:13602–13607.
4. Guo H, Bueler SA, Rubinstein JL (2017) Atomic model for the dimeric F_O region of mitochondrial ATP synthase. *Science* 358:936–940.
5. Lapaille M, et al. (2010) Atypical subunit composition of the chlorophycean mitochondrial F_1F_O-ATP synthase and role of Asa7 protein in stability and oligomycin resistance of the enzyme. *Mol Biol Evol* 27:1630–1644.
6. Paumard P, et al. (2002) The ATP synthase is involved in generating mitochondrial cristae morphology. *EMBO J* 21:221–230.
7. Arselin G, et al. (2004) The modulation in subunits e and g amounts of yeast ATP synthase modifies mitochondrial cristae morphology. *J Biol Chem* 279:40392–40399.
8. Minauro-Sanmiguel F, Wilkens S, García JJ (2005) Structure of dimeric mitochondrial ATP synthase: Novel F_0 bridging features and the structural basis of mitochondrial cristae biogenesis. *Proc Natl Acad Sci USA* 102:12356–12358.
9. Dudkina NV, Heinemeyer J, Keegstra W, Boekema EJ, Braun HP (2005) Structure of dimeric ATP synthase from mitochondria: An angular association of monomers induces the strong curvature of the inner membrane. *FEBS Lett* 579:5769–5772.
10. Dudkina NV, Sunderhaus S, Braun HP, Boekema EJ (2006) Characterization of dimeric ATP synthase and cristae membrane ultrastructure from *Saccharomyces* and *Polytomella* mitochondria. *FEBS Lett* 580:3427–3432.
11. Allen RD (1995) Membrane tubulation and proton pumps. *Protoplasma* 189:1–8.
12. Strauss M, Hofhaus G, Schröder RR, Kühlbrandt W (2008) Dimer ribbons of ATP synthase shape the inner mitochondrial membrane. *EMBO J* 27:1154–1160.
13. Davies KM, et al. (2011) Macromolecular organization of ATP synthase and complex I in whole mitochondria. *Proc Natl Acad Sci USA* 108:14121–14126.
14. Dudkina NV, Oostergetel GT, Lewejohann D, Braun HP, Boekema EJ (2010) Row-like organization of ATP synthase in intact mitochondria determined by cryo-electron tomography. *Biochim Biophys Acta* 1797:272–277.

15. Mühleip AW, et al. (2016) Helical arrays of U-shaped ATP synthase dimers form tubular cristae in ciliate mitochondria. *Proc Natl Acad Sci USA* 113:8442–8447.
16. Mühleip AW, Dewar CE, Schnaufer A, Kühlbrandt W, Davies KM (2017) In situ structure of trypanosomal ATP synthase dimer reveals a unique arrangement of catalytic subunits. *Proc Natl Acad Sci USA* 114:992–997.
17. Hahn A, et al. (2016) Structure of a complete ATP synthase dimer reveals the molecular basis of inner mitochondrial membrane morphology. *Mol Cell* 63:445–456.
18. Klusch N, Murphy BJ, Mills DJ, Yildiz Ö, Kühlbrandt W (2017) Structural basis of proton translocation and force generation in mitochondrial ATP synthase. *eLife* 6: e33274.
19. Srivastava AP, et al. (2018) High-resolution cryo-EM analysis of the yeast ATP synthase in a lipid membrane. *Science* 360:eaas9699.
20. Anselmi C, Davies KM, Faraldo-Gómez JD (2018) –Mitochondrial ATP synthase dimers spontaneously associate due to a long-range membrane-induced force. *J Gen Physiol* 150:763–770.
21. Althoff T, Davies KM, Schulze S, Joos F, Kühlbrandt W (2012) GRecon: A method for the lipid reconstitution of membrane proteins. *Angew Chem Int Ed Engl* 51: 8343–8347.
22. Allegretti M, et al. (2015) Horizontal membrane-intrinsic α-helices in the stator a-subunit of an F-type ATP synthase. *Nature* 521:237–240.
23. Couoh-Cardel SJ, Uribe-Carvajal S, Wilkens S, García-Trejo JJ (2010) Structure of dimeric F_1F_0-ATP synthase. *J Biol Chem* 285:36447–36455.
24. Thomas D, et al. (2008) Supramolecular organization of the yeast F_1F_o-ATP synthase. *Biol Cell* 100:591–601.
25. Arnold I, Pfeiffer K, Neupert W, Stuart RA, Schägger H (1999) ATP synthase of yeast mitochondria. Isolation of subunit j and disruption of the ATP18 gene. *J Biol Chem* 274:36–40.
26. Baker LA, Watt IN, Runswick MJ, Walker JE, Rubinstein JL (2012) Arrangement of subunits in intact mammalian mitochondrial ATP synthase determined by cryo-EM. *Proc Natl Acad Sci USA* 109:11675–11680.
27. Jiko C, et al. (2015) Bovine F_1F_o ATP synthase monomers bend the lipid bilayer in 2D membrane crystals. *eLife* 4:e06119.
28. Kahraman O, Stoop N, Müller MM (2012) Morphogenesis of membrane invaginations in spherical confinement. *Europhys Lett* 97:68008.
29. Renken C, et al. (2002) A thermodynamic model describing the nature of the crista junction: A structural motif in the mitochondrion. *J Struct Biol* 138:137–144.
30. Brandt T, et al. (2017) Changes of mitochondrial ultrastructure and function during ageing in mice and *Drosophila*. *eLife* 6:e24662.
31. Rieger B, Junge W, Busch KB (2014) Lateral pH gradient between OXPHOS complex IV and F_0F_1 ATP-synthase in folded mitochondrial membranes. *Nat Commun* 5:3103.
32. Atteia A, van Lis R, Ramírez J, González-Halphen D (2000) Polytomella spp. growth on ethanol. Extracellular pH affects the accumulation of mitochondrial cytochrome c550. *Eur J Biochem* 267:2850–2858.
33. Vazquez-Acevedo M, et al. (2006) The mitochondrial ATP synthase of chlorophycean algae contains eight subunits of unknown origin involved in the formation of an atypical stator-stalk and in the dimerization of the complex. *J Bioenerg Biomembr* 38: 271–282.
34. Davies KM, et al. (2014) Visualization of ATP synthase dimers in mitochondria by electron cryo-tomography. *J Vis Exp,* 51228.
35. Kremer JR, Mastronarde DN, McIntosh JR (1996) Computer visualization of three-dimensional image data using IMOD. *J Struct Biol* 116:71–76.
36. Pruggnaller S, Mayr M, Frangakis AS (2008) A visualization and segmentation toolbox for electron microscopy. *J Struct Biol* 164:161–165.